Hindawi
International Journal of Photoenergy
Volume 2019, Article ID 1540271, 11 pages
https://doi.org/10.1155/2019/1540271

*Research Article*

# Photocatalytic Degradation of 2,4-Dichlorophenol by $TiO_2$ Intercalated Talc Nanocomposite

**Manqing Ai, Wenli Qin, Tian Xia, Ying Ye, Xuegang Chen, and Pingping Zhang**

*Zhejiang University, Marine Science Department, Zhoushan 316000, China*

Correspondence should be addressed to Pingping Zhang; marin011@qq.com

Received 12 October 2018; Revised 11 January 2019; Accepted 4 February 2019; Published 3 March 2019

Academic Editor: K. R. Justin Thomas



Novel nanocomposites have been prepared by intercalating $TiO_2$ nanoparticles into talc. The nanocomposites have been verified by X-ray diffraction (XRD) from the appearance of a characteristic diffraction peak of $TiO_2$. Thermal behavior of the prepared samples is examined by thermogravimetric analyzer (TGA), scanning electron microscope (SEM), and energy dispersive spectrometer (EDS), which have shown no $TiO_2$ particles on the surface of the talc. The $TiO_2$ particles are found in the layers of talc by transmission electron microscopy (TEM) and the Brunauer-Emmett-Teller (BET) method, which have shown the increase of specific surface areas and total pore volumes and the decline of average pore diameters. As the strong adsorption ability of talc can intensify the power of photon absorption and capture-recombination carriers, more than 99.5% of 2,4-dichlorophenol can be degraded in 1 h by the nanocomposite under an ultraviolet lamp in neutral solution and room temperature after reaching adsorption equilibrium, and the result of adsorbance is in accord with the first-order kinetic. The degradation rate was maintained at about 99% after 20 times. Therefore, the prepared talc/$TiO_2$ nanocomposite is an efficient, stable, and recyclable material for wastewater treatment.

## 1. Introduction

Phenolic compounds have been widely used in industrial and agricultural manufacture and are ranked as one of the most harmful and extensive organic contaminants [1]. Among the phenolic compounds, the chlorophenols can cause deterioration of water quality and may threaten human health and survival of other organisms [2, 3]. As one of the most widely used chlorophenols, 2,4-dichlorophenol (2,4-DCP) can produce hazardous secondary pollution [4–9]. It has been demonstrated that while 2,4-DCP can be decomposed by a variety of methods, the degradation efficiency is low. For example, Luo et al. have shown that 6.8 mg 2,4-DCP was degraded by ZnO in 1 h in UV light [10]; Li et al. have shown that 29 mg 2,4-DCP was degraded by nanobamboo charcoal in 1 h [2]; Mohammadi and Sabbaghi prepared MWCNT (multiwall carbon nanotubes)/$TiO_2$ which takes 2 hours to transform about 47 mg 2,4-DCP into harmless substance in 1 L alkaline solution [11]; Yang and coworkers made $TiO_2$ film which degrades only about 5.5 mg 2,4-DCP in 2 hours [12]. So a safe, efficient, and environment friendly way to degrade 2,4-DCP is required.

$TiO_2$ has superior photocatalytic performance due to its strong oxidizing ability, nontoxicity, and long-term stability of photochemistry [12–17]. Among the various crystalline structures of $TiO_2$, anatase is confirmed to be the most active photocatalyst, which has been a research focus to degrade the pollutants therefore [18]. Medical talc also possesses the characteristics of talc such as chemical stability, good flame resistance, and strong adsorption and is shiny white, nontoxic, and nonpolluting after undergoing purification from raw talc [19–22]. Talc can intensify the power of photon absorption and capture-recombination carriers due to its strong adsorption ability, which may thus improve the photocatalysis of $TiO_2$ [16]. Talc has been used to produce a kind of nanocomposite to degrade dye [23], and talcum powder is in widespread use in plastics and coatings [24–26]. These show that talc can improve the efficiency of photodegradation of 2,4-DCP and reduce the cost of wastewater treatment when used in the production of plastics or metal coatings.

In order to improve the purification efficiency of wastewater and promote the application of the talc in photocatalysis, we prepared $TiO_2$/medical talc nanocomposites under two different temperature conditions through the full-scan UV–Vis absorption spectra and total organic carbon (TOC) analyzer, establishing whether the benzene ring was decomposed and confirming that 2,4-DCP was mineralized into inorganic substances. Finally, the photocatalytic stability of the nanocomposite was verified by repeated trails.

## 2. Materials and Method

*2.1. Chemical and Materials.* Medical talc obtained from talc powder plant of You County, Hunan Province, China, with a particle size of 38 $\mu$m, was used without further purification. Tetrabutyl titanate (TNBT) was purchased from Aladdin Industrial Co., Ltd., Shanghai, China. Absolute ethyl alcohol (analytical reagent grade) and 2,4-dichlorophenol (2,4-DCP, ≥99%) were purchased from Sinopharm Chemical Reagent Co., Ltd., Shanghai, China. Deionized water with a resistivity of 18.2 mΩ was used for preparing aqueous solutions.

*2.2. Preparation of $TiO_2$-Medical Talc Nanocomposites.* The medical talc (50 g) was dried at 80°C for 8 h and was marked as MT. TNBT solution was added dropwise into absolute ethanol with stirring for 2 h; distilled water was added into the mixture dropwise until there was no sedimentation. The obtained product was named as HTO.

50 g of TNBT solution was mixed with 10 g of MT in a mortar, and the mixture ground till it became pasty, and dried after cleaning to acquire intercalating composite, T-H. All three samples were calcined at 400°C for 2 h at a heating rate of 2°C $min^{-1}$. The products were labeled as T-400, H-400, and T-H-400, respectively, [23]. The sample list is shown in Table 1.

*2.3. Characterization.* X-ray diffraction (XRD) spectra of samples were examined by a Rigaku D/Max 2550 X-ray Diffractometer (Japan) using Cu Kα radiation ($\lambda = 0.15418$ nm) at 450 mA and 60 kV. Thermal behavior of the prepared samples was examined by thermogravimetric analyzer (TGA) model Precisa DSC3+ (Switzerland) from 50°C to 700°C. The microstructures and the energy dispersive spectra (EDS) of the samples were observed through an SU-8010 scanning electron microscope (SEM, Japan). The microstructures of the samples were observed using transmission electron microscopy (TEM) (JEM-2100PLUS, JEOJ). The BET surface area and pore characteristics were analyzed by using nitrogen adsorption-desorption (AUTOSORB-IQ-MP, USA) at 77 K. The total organic carbon (TOC) content was analyzed by ASI-L TOC analyzer (Shimadzu, Japan).

*2.4. Photocatalytic Performance.* For the adsorption experiment, the mixture (50 ppm 2,4-DCP solution and 2 g·$L^{-1}$ sample) was stirred vigorously in darkness. After 25 min, the platform of 2,4-DCP solution removal was reached indicating that an adsorption/desorption equilibrium has been achieved. The mixture was then irradiated with a 250 W high-pressure mercury ultraviolet (UV) lamp (main emission wavelength: 365 nm, intensity: 327.3 kJ·$mol^{-1}$, Shenzhen Guyou Special Light Source Co., Ltd., China) for certain times. After the UV irradiation, the mixture was centrifuged, and its absorbance was analyzed by using a UV–Vis spectrophotometer (Shimadzu UV-2550, Japan) at a wavelength of 283 nm [12], and the degraded solution was analyzed by ASI-L TOC analyzer (Shimadzu, Japan). The repeated trials proceeded at the same condition: add 2 g $L^{-1}$ T-H-400 into the initial 50 ppm 2,4-DCP solution, turn on the UV lamp after reaching the adsorption equilibrium, and photodegrade the initial solution for 1 h, then obtain the liquid sample and dry the T-H-400 for the next repetitive degradation. Removal rate and relative removal rate are calculated according to the following equations:

$$\text{Removal rate}\,(\%) = \frac{C_0 - C_a}{C_0} * 100\%, \quad (1)$$

$$\text{Relative removal rate}\,(\%) = \frac{C_b - C_c}{C_b} * 100\%, \quad (2)$$

where $C_0$, $C_a$, $C_b$, and $C_c$ are the initial 2,4-DCP concentration, the 2,4-DCP concentration after degradation, the 2,4-DCP concentration after adsorption under dark, and the 2,4-DCP concentration after photodegradation, respectively. All experiments were carried out three times, and the average values and standard errors were then used.

Table 1: The list of samples that were prepared during each stage.

| Name | Treatment |
|---|---|
| MT | Medical talc |
| HTO | Hydrolyzing $TiO_2$ |
| T-H | Intercalation of TNBT into talc |
| T-400 | Calcined MT at 400°C |
| H-400 | Calcined HTO at 400°C |
| T-H-400 | Calcined TH at 400°C |

## 3. Results and Discussion

*3.1. Characterization of the $TiO_2$/Medical Talc Nanocomposite.* Figure 1 shows the XRD spectra of the samples. From the XRD results of MT and T-400, shown in Figures 1(a) and 1(b), respectively, we found that after calcination, the crystallite size increased slightly (MT: 337 nm, T-400: 374 nm). The difference between MT and T-400 suggests that the calcination reduced the crystallinity of the talc, although the reduction was not significant. The weak characteristic peak of anatase appeared at 2 $\theta = 25.4°$ in the HTO which indicates that the $TiO_2$ has been generated after hydrolyzing the TNBT [27–30]. As the temperature of the calcination rose, the crystallite size increased in H-400 (HTO: 86 nm, H-400: 124 nm), which means the crystallinity of anatase was improved. Comparing the ratios of the intensity peaks of MT and T-H at 2 $\theta = 9.4°$ and 28.6°, the ratio has declined (MT: 0.599, T-H: 0.261), which indicates the number of crystal lattices has decreased in the talc, due to the insertion of $TiO_2$ (diameter 5 nm) between the layers of the

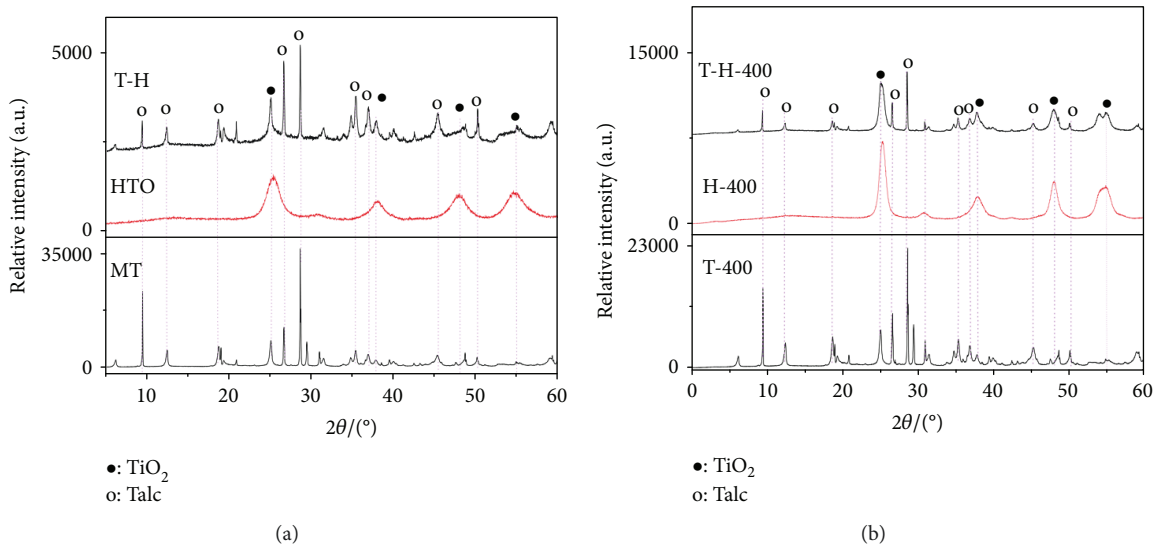


Figure 1: XRD spectra of samples ((a) XRD spectra of samples: MT, HTO, and T-H; (b) XRD spectra of samples: T-400, H-400, and T-H-400).

talc lattice. The crystallite size of T-H also declined to 273 nm compared with MT. After calcination, the T-H-400 has similar variation with T-H compared with T-400; it has also decreased the ratios of the intensity peaks of T-400 and T-H-400 at 2t $\theta = 9.4^{\circ}$ and $28.6^{\circ}$ (T-400: 0626, T-H-400: 0.353), and the crystallite size of T-H-400 also declined to 142 nm compared with T-400 [31, 32]. From the results, it can be concluded that, by the reason of the lower atomic radius of $TiO_2$, the number of crystal lattices decreased in the talc when $TiO_2$ is inserted into the layers of talc, and there is no chemical reaction when intercalating the $TiO_2$ into the medical talc [33, 34].

Figure 2 shows the TG curves of all samples. The thermogram can be divided into three stages. In the first stage, there is a heat release from all samples, due to the evaporation of bound water (desorption of water physically bound to the surface), around 60°C to 80°C. The second stage is divided into two kinds of behavior, depending on the nature of the sample: one kind is around 240°C to 260°C; there are distinct heat release peaks in the two kinds of $TiO_2$ (HTO and H-400) and nanocomposites (T-H and T-H-400), generated by the oxidation of TNBT and other hydrolytic organic matter (the residue during the preparation of samples); the other kind of behavior is due to two types of talc (MT and T-400) and nanocomposites; the small but discernible heat release is at about 510°C (nanocomposites) and 560°C (talc), due to the evaporation of bound water which exists in the layers of talc. The third stage is also divided similarly to the second stage: the first kind of behavior relates to the two kinds of $TiO_2$ and nanocomposites, with a weak heat release peak around 540°C to 580°C, ascribed to the lattice deformation of $TiO_2$; the second is attributed to the oxidation of hydroxide radical of talc; subtle heat release peak shows up around 580°C to 590°C [35, 36].

The morphology of samples is displayed in Figures 3 and 4. The SEM pattern of MT and T-400 (Figures 3(a) and 3(b)) reveals that the medical talc has laminar structure and the

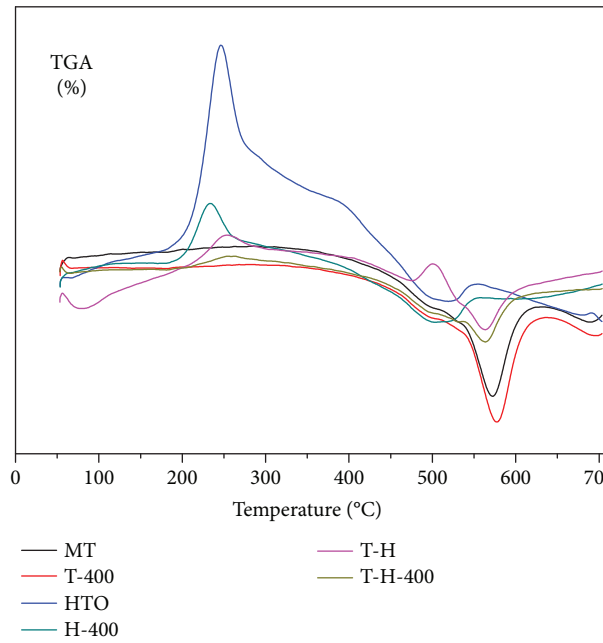


Figure 2: TG curves of all samples.

layers are more compact in the T-400 compared with MT because high temperature can cause expansion of the laminar structure. Figures 3(c) and 3(d) depict the SEM patterns of HTO and H-400; the result shows that the laminar structure has appeared in H-400, which is different from HTO which has globular structure. Also, H-400 has a better degree of crystallinity which benefits from the reinforcement by the crystal structure of anatase [21]. Figures 4(a)–4(d) depict the SEM patterns of T-H and T-H-400, respectively, at different magnifications; few globular features due to $TiO_2$ appear on the surface of the layer, indicating that most of the $TiO_2$ is intercalated within the talc lattice.

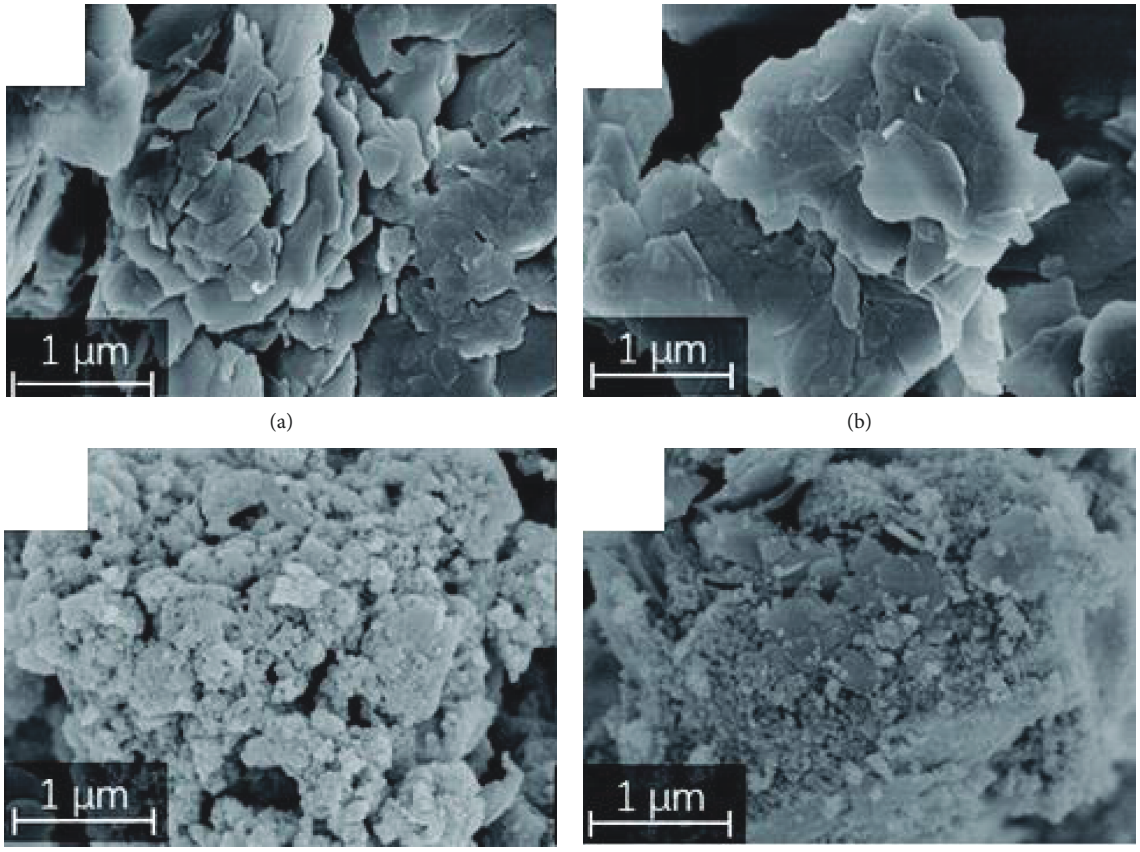


Figure 3: SEM images of (a) medical talc (MT), (b) medical talc after calcining at 400°C (T-400), (c) hydrolyzing $TiO_2$ (HTO), and (d) $TiO_2$ after calcining at 400°C (H-400).

Figure 5 represents the EDS spectrum of the nanocomposites. From the results, we find that the content of Ti is 0.73% in the T-H and 13.73% by weight in the T-H-400. The maldistribution of $TiO_2$ in the layer of talc contributes to the different content of Ti in the composites. Comparing with the results of SEM, there is little $TiO_2$ on the surface of layers of medical talc; hence, we can conclude that the nanocomposites have been prepared successfully.

The microstructures of the samples are shown in Figure 6. We find no distinct difference between MT and T-400 (regular laminar structure without globular nanoparticles), conforming with the results of XRD and SEM. After intercalating the $TiO_2$, there are many tiny $TiO_2$ nanoparticles (about 6 nm) without different kind of lattice fringe in the TEM image of nanocomposites, shown in Figures 6(c) and 6(d), indicating that the $TiO_2$ particles exist between layers and not on the surface of talc. More important, the obvious lattice fringe can be found in Figure 6(d), indicating that the samples possess high crystallinity. Photocatalytic activity of talc is expected to be enhanced by the uniform dispersion of $TiO_2$ nanoparticles in the layers of talc [28]. This is consistent with the XRD and SEM results and suggests that the $TiO_2$ has intercalated into the layers of talc.

Figure 7(a) shows the nitrogen adsorption-desorption isotherms of all samples. According to the hysteresis loops and curves, the nitrogen sorption curves of talc (MT and T-400) and $TiO_2$ (HTO and H-400) show type III and type V isotherm, respectively [37]. When the talc was intercalated with $TiO_2$, the isotherm type then changed to type V and the type of hysteresis loop which is H3 appeared (T-H and T-H-400) [38]. The changes represent the intercalation of $TiO_2$ nanoparticles within the layers of talc that has formed slit-type holes. From the pore diameter distribution curves of all samples shown in Figure 5(b), the dominant pore diameters of T-H and T-H-400 have changed to 6 nm and 8 nm, while the mesopores (>15 nm) have disappeared compared with MT and T-400. The changes of nanocomposites are due to the insertion of $TiO_2$, which has lower pore diameters between layers of talc.

The specific surface areas ($S_{BET}$), total pore volumes ($V_t$), and average pore diameter ($d$) of the samples are listed in Table 2. From the results, after calcination, there are slight changes in T-400 and H-400, compared with MT and HTO, respectively, which may result in their similar adsorption performance. However, after calcination, T-H-400 has larger average pore diameter (9.10 m) than T-H (2.74 nm) while their total pore volumes are similar, and this may contribute to the higher adsorption capacity of T-H-400 [23]. On account of the intercalation of $TiO_2$, the $S_{BET}$ and $V_t$ of nanocomposites (T-H and T-H-400) have increased and the

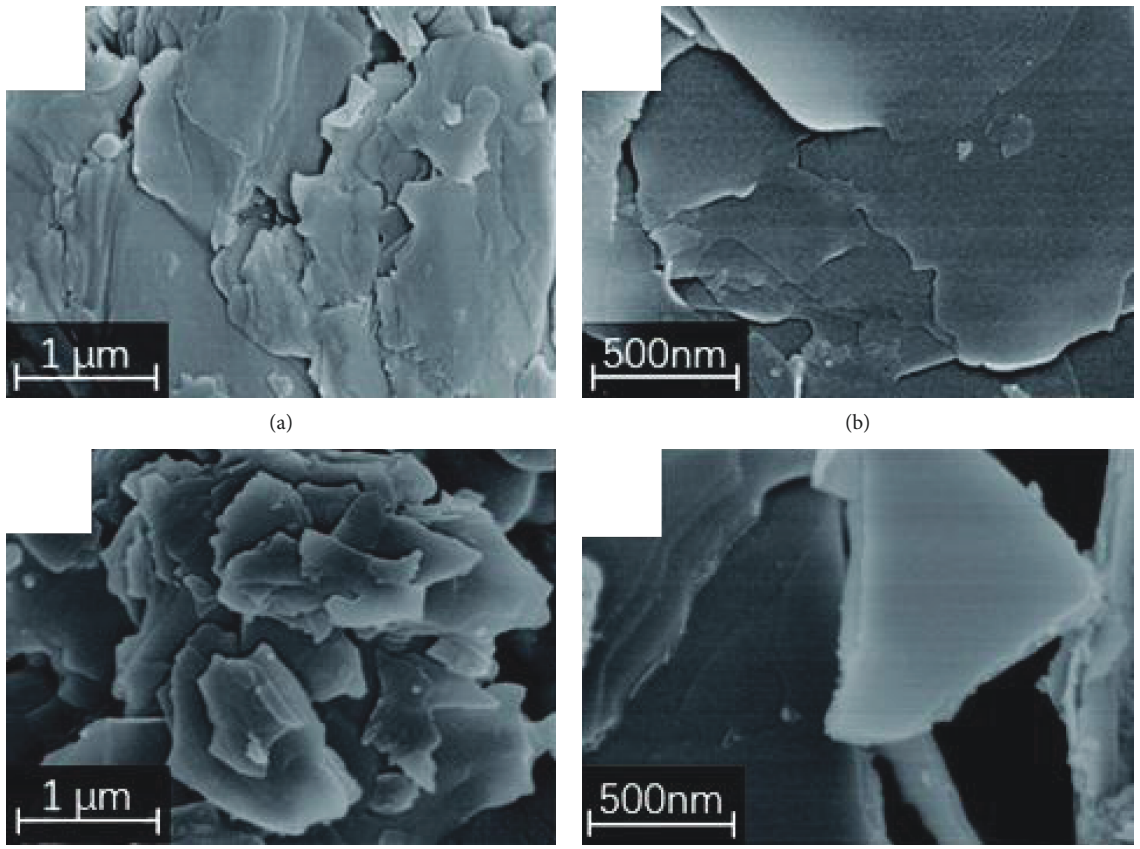


(a) (b) (c) (d)

Figure 4: SEM images of (a, b) medical talc intercalated with TNBT (T-H) and (c, d) medical talc intercalated with TNBT after calcining at 400°C (T-H-400).

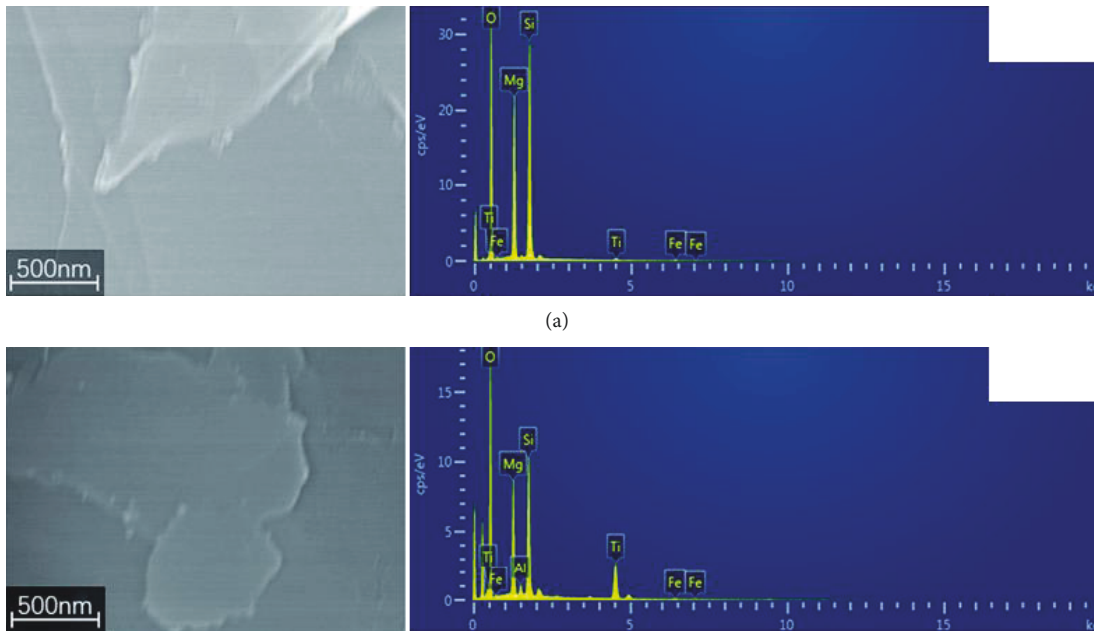


(a)

(b)

Figure 5: EDS spectrum of the nanocomposites ((a) T-H; (b) T-H-400).

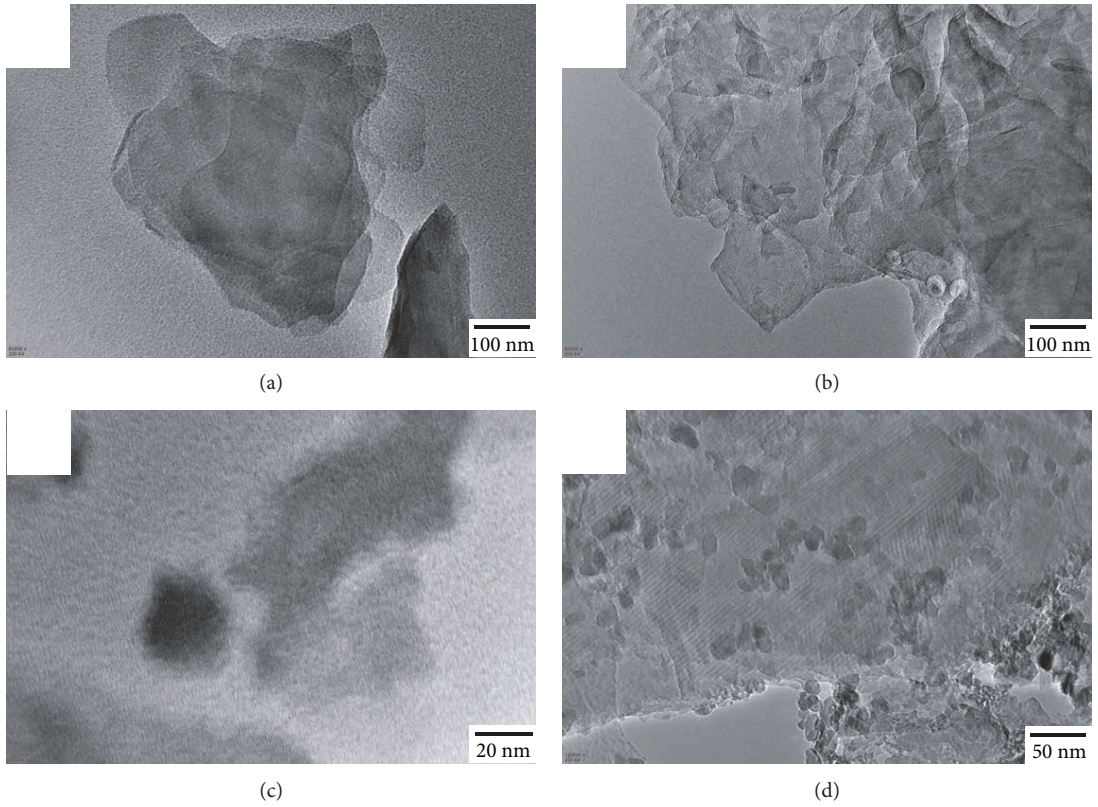


Figure 6: TEM images of all samples ((a) MT; (b) T-400; (c) T-H; (d) T-H-400).

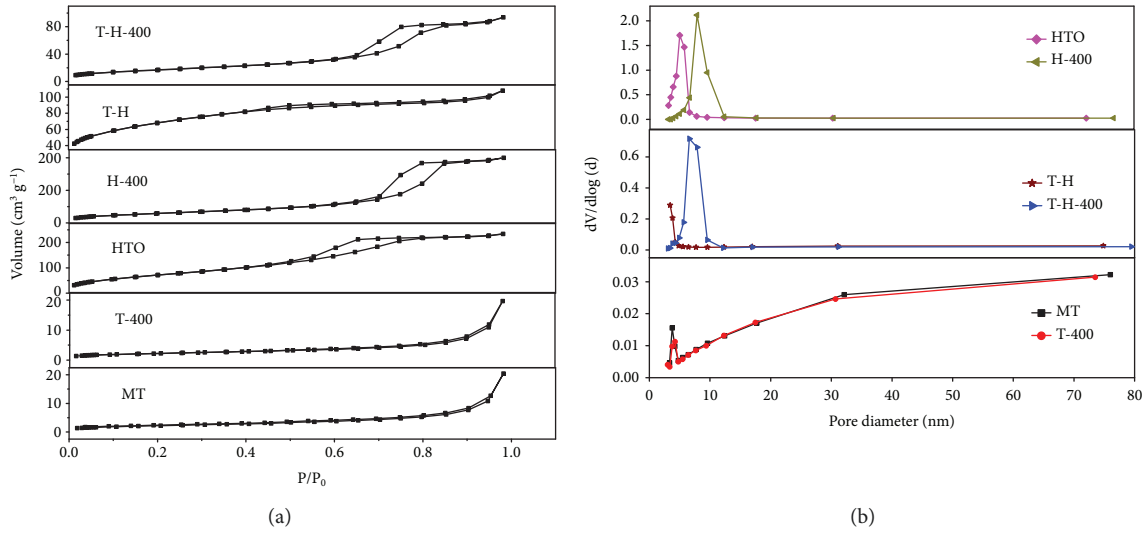


Figure 7: (a) Nitrogen adsorption-desorption isotherms for all samples; (b) pore diameter distribution curves of all samples.

average pore diameter has declined compared with talc (MT and T-400), which may result in a decrease of the adsorption capacity. As a result, the differences in BET between talc and nanocomposites can further verify that the $TiO_2$ has been intercalated into talc successfully.

*3.2. Photocatalytic Performance.* In order to examine the photocatalytic degradation capacities of the $TiO_2$/medical talc for 2,4-DCP, all samples were tested in the dark to first obtain the adsorption data. The plateau of adsorptions of the 2,4-DCP of all samples was reached after 25 min, indicating that they have reached the adsorption equilibrium. From Figure 8, the maximum adsorption rates were 77.8% for MT and 75.6% for T-400 due to their larger average pore diameters. Sample HTO showed better adsorption ability than H-400 due to its larger specific surface area and total pore volume.

Table 2: Specific surface area ($S_{BET}$) of the samples.

| Sample | $S_{BET}$ ($m^2 \cdot g^{-1}$) | $V_t$ ($cm^3 \cdot g^{-1}$) | $d$ (nm) |
|---|---|---|---|
| MT | 7.92 | 0.032 | 15.98 |
| T-400 | 8.03 | 0.030 | 15.13 |
| HTO | 280.69 | 0.36 | 5.16 |
| H-400 | 112.06 | 0.31 | 11.04 |
| T-H | 244.07 | 0.17 | 2.74 |
| T-H-400 | 63.59 | 0.14 | 9.10 |

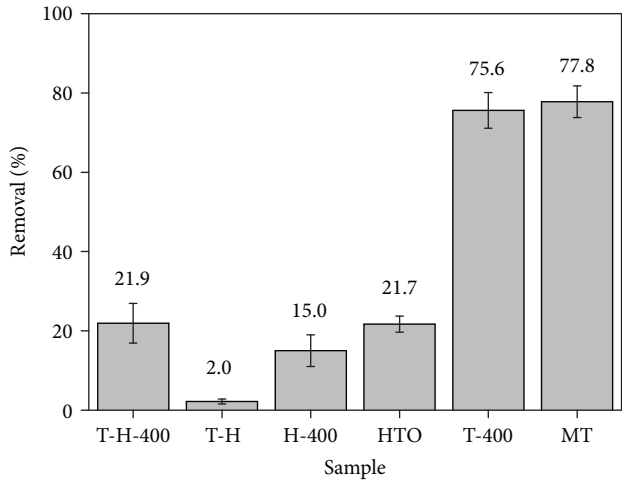


Figure 8: The effect of the adsorption on the degradation of 2,4-DCP solution by all samples in the dark.

Sample T-H has lower adsorption rate, being only 2%, compared to 21.9% for T-H-400, because of its lower average pore diameters and the larger atom of 2,4-DCP, corresponding with the result in Figure 5(b) and Table 2 (almost all pore diameters of T-H are smaller than 3 nm).

Figure 9 denotes the full-scan UV–Vis absorption spectrums of 2,4-DCP solution after treatments by all samples. After arriving the adsorption equilibrium, the absorption peak of 2,4-DCP has changed from 283 nm to 243 nm by MT and T-400 in the dark. The blue shift may be caused by the decrease of pH in the solution, as the 2,4-DCP is low-acid ion compound, and the $H^+$ of 2,4-DCP in the solution has increased with the proceed of adsorption. Another reason may be because the –Cl has dropped off the ben zing, the generation of phenol, or other organics with ben zing [24, 39, 40]. When the $TiO_2$ intercalated into the layers of talc, there is great removal of 2,4-DCP without blue shift at 283 nm, which means that the pollutants were not only physical adsorption but also were degraded, even though, it cannot reach the environmental target.

From the results shown in Figures 8 and 9, it can be concluded that without the addition of photocatalysis, adsorption capacity of medical talc, $TiO_2$, and nanocomposites cannot achieve the target of degrading most of the pollutant without secondary pollution in a short time [41].

After reaching the adsorption equilibrium, the UV lamp was turned on to examine the photocatalytic performance

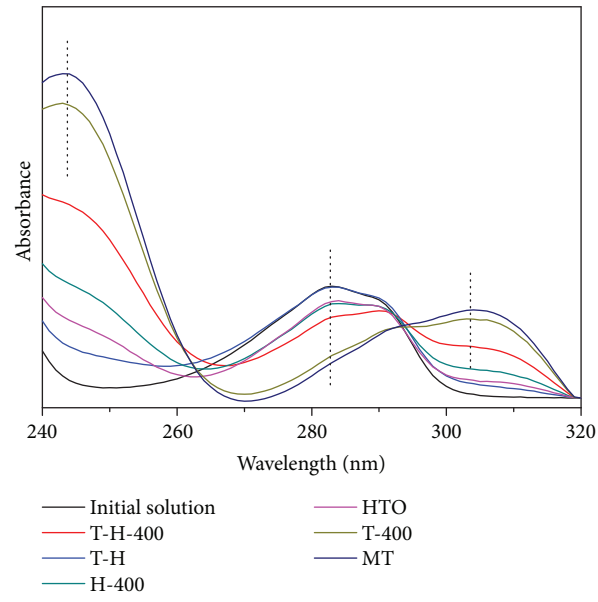


Figure 9: Full-scan UV–Vis absorption spectrums of 2,4-DCP solution after treatments by all samples. Initial 2,4-DCP concentration: 50 mg $L^{-1}$.

of the samples. From Figure 10, which shows the photodegradation rate of 2,4-DCP solution in 1 h for all samples, the MT and T-400 appear the alike in photocatalytic capacity; however, the relative removal rate is negative because of the red shift in the characteristic peak of 2,4-DCP shown in Figure 10. The H-400 has higher degradation rate -82.5% compared with 59.3% for HTO, attributed to the better anatase structure. The degradation rates of T-H and T-H-400 are 66.3% and 99.5%, respectively, and they have better photocatalytic power than talc (MT and T-400) and $TiO_2$ (HTO and H-400) at the same temperature. Among all the samples, the maximum 2,4-DCP removal rate was generated by T-H-400.

Figure 11 shows the full-scan UV–Vis absorption spectra of 2,4-DCP solutions after treatments by all samples for 1 h, and the absorption peak has changed from 243 nm to 255 nm compared with the characteristic peak of 2,4-DCP concentration after absorption by MT and T-400. The red shift is because the temperature of solution has increased with the lighting of lamp, and the pH has increased due to the combination of $H^+$ and $C_6H_6Cl_2O^-$[24, 40]. In summary, the photodegradation of the medical talc fails to achieve the expectation which will not cause secondary pollutant.

Apart from the medical talc, which has little or no photocatalytic ability on its own, the time dependence of the removal rates of the 2,4-DCP by T-H-400, T-H, H-400, and HTO are shown in Figure 12. Initially, there was a slight decrease in removal by T-H because of the effect of the evaporation of the water and the desorption of the material, whereas the degradation rates of other three samples increased continuously. From 40 min to 60 min, the T-H showed a major increase in the degradation of the pollutant, while H-400 was surpassed and became the last one. The leap is because the 2,4-DCP solution began to degrade under the

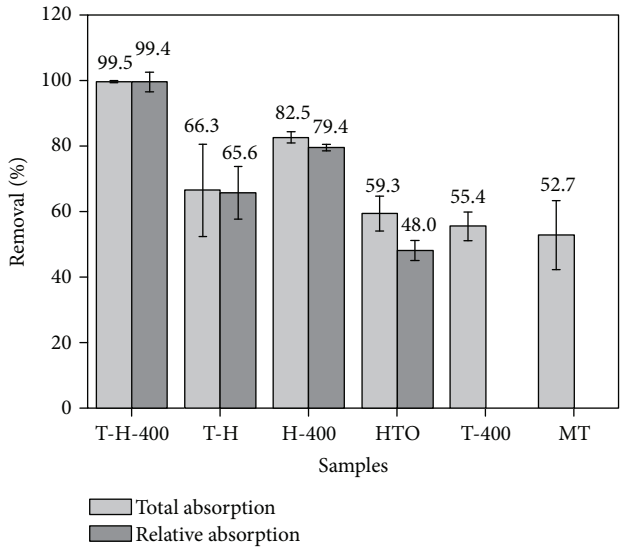


Figure 10: Photodegradation rate of 2,4-DCP solution for 1 h by all materials. Total absorption is in accordance with equation (1). Relative absorption is in accordance with equation (2).

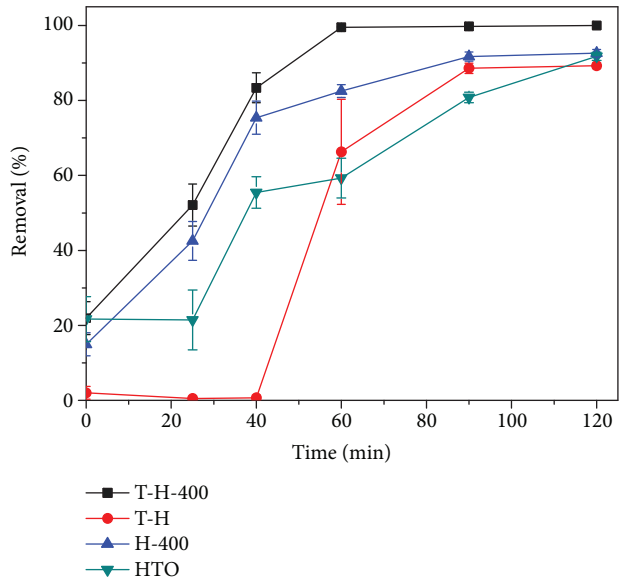


Figure 12: The change of the removal rate of the 2,4-DCP by T-H, T-H-400, H-400, and HTO.

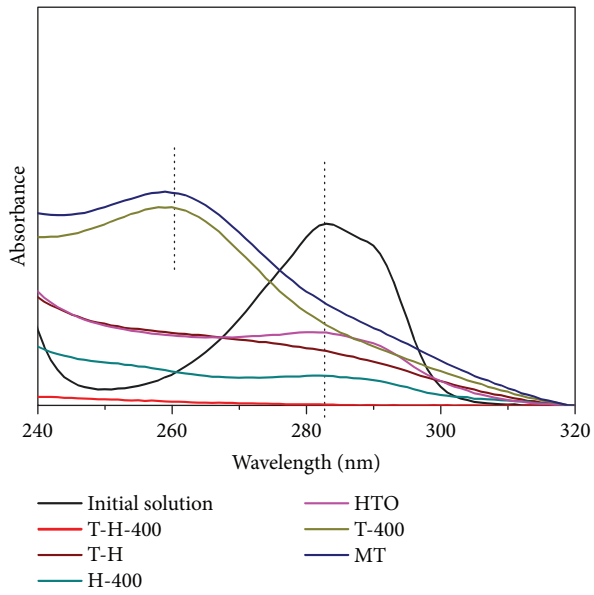


Figure 11: The full-scan UV–Vis absorption spectra of 2,4-DCP solutions for all samples after photodegradation by for 1 h.

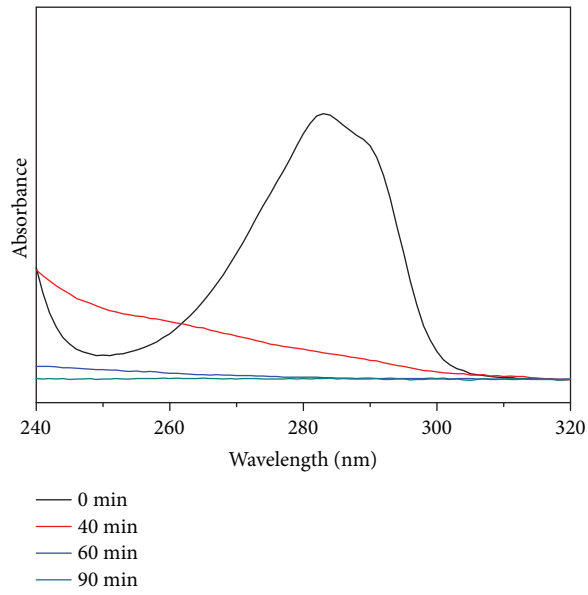


Figure 13: Full-scan UV–Vis absorption spectrums of 2,4-DCP solutions after treatments by T-H-400 for 0 min, 40 min, 60 min, and 90 min.

UV lamp without photocatalysis, which resulted in a blue shift of the absorption peak (from 283 nm to 222 nm); similar with the dark adsorption of talc, there is generation of phenol or other aromatics [1]. From 60 min to the end of the experiment, the total degradation of T-H-400 increased from 99.5% to 100% slightly; the second one is the total degradation of H-400 which increased from 82.5% to 92.6%. Overall, T-H-400 showed the best photocatalytic performance.

Figure 13 shows the full-scan UV–Vis absorption spectra of 2,4-DCP solution after treatments by T-H-400. The absorption peak value at 283 nm decreased over time, and the peak disappeared in 60 min. After 60 min, the absorption spectra of 2,4-DCP solution was close to a line without the peaks representing the benzene ring.

It has been measured for the total oxygen carbon of the initial 2,4-DCP concentration and the 2,4-DCP concentration after treatment by T-H-400 under UV lamp for 2 h. The NPOC declined from 16.04 mg·$L^{-1}$ to 0.91 mg·$L^{-1}$ which is positively correlated with the concentration of TOC in the solution, indicating that the benzene rings in the 2,4-DCP have been almost completely broken down. Compared with the result shown in Figure 11, we can conclude

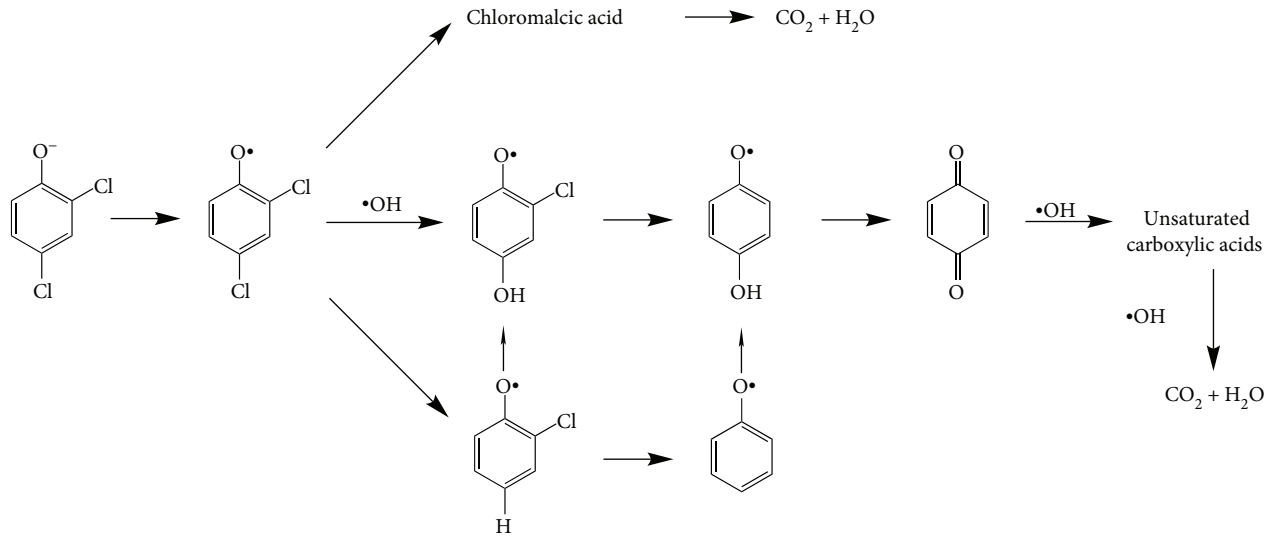


Figure 14: The pathway of decomposition of 2,4-DCP.

that a part of 2,4-DCP has been mineralized to $CO_2$, $H_2O$, and ions [42].

From the proposed pathway for 2,4-DCP degradation by TiO2/medical talc which has been investigated [3, 8–10, 42], we can summarize as follows: medical talc not only has high absorption capacity but also can enhance the power of photon absorption and capture-recombination carriers; therefore, medical talc has increased the photon utilization for $TiO_2$. Also in T-H-400, there is synergy between $TiO_2$ and medical talc in photocatalysis. As a result, the photocatalytic power of $TiO_2$ has been intensified significantly, and nanocomposite T-H-400 can mineralize the pollutant in a short time. The pathway of the decomposition of 2,4-DCP is effected through the bombarding of $OH^{\cdot}$, through which the benzene ring is disassembled. Finally, the 2,4-DCP is mineralized to $CO_2$, $H_2O$, and ions (chloride and others) (Figure 14).

In order to establish the stability of photocatalytic degradation, the T-H-400 has been recycled 20 times to photodegrade the initial 2,4-DCP solution under the UV lamp for 1 h after 25 min in the dark, and the result is shown in Figure 15. From Figure 15, the removal rate is about 99% in spite of few fluctuation, and the sample standard deviation is only 0.0037 according to equation (3). The nanocomposite shows the excellent photocatalytic stability for decomposing the 2,4-DCP, which will extend the photocatalytic life in the practical application. Consequently, the T-H-400 nanocomposite is a sustainable and recyclable material for photocatalytic degradation of 2,4-DCP.

$$S = \sqrt{\frac{1}{N-1}\sum_{i=1}^{N}\left(X_i - \check{X}\right)^2}, \quad (3)$$

where $S$, $N$, $X$, and $\check{X}$ are the sample standard deviation, the repeated times, and sample average, respectively.

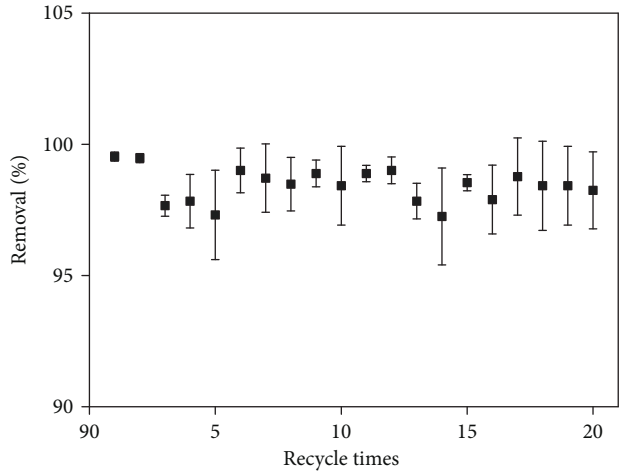


Figure 15: The removal rate of the initial 2,4-DCP solution by T-H-400 under the UV lamp for 1 h after 25 min in the dark.

## 4. Conclusions

The 99.5% decomposition of the pollutant can be achieved in 1 h. The optimum condition is in neutral aqueous solution at room temperature under a UV lamp. This clearly enhances the photocatalytic capacity of $TiO_2$. The excellent photocatalytic performance can be achieved by a few of nanocomposites. The degree of degradation can be maintained at about 99% after 20 iterations with the same nanocomposite material.

In situ formation of $TiO_2$ nanoparticles in the layers of medical talc thus has marked effect on the purification of the initial solution, indicating that medical talc can significantly enhance the photocatalytic activity of $TiO_2$. This remarkable photocatalytic power will promote the potential applications of medical talc in wastewater treatment.

## Data Availability

The data used to support the findings of this study are included within the article.

## Conflicts of Interest

The authors declare that they have no conflicts of interest.

## Acknowledgments

We thank Professor Benjamin Kneller for polishing the manuscript. This work has been supported by the National Oil and Gas Project 529000-RE1201.

## References

[1] L. Ge, Z. Zhang, F. Wu, and N. Deng, "Photolysis of 2,4-Dichlorophenol in Water," *Environmental Science and Technology*, vol. 27, 2004.

[2] X. Li, Y. Yue, R. Hua et al., "Photocatalytic Degradation of 2,4-dichlorophenol in Aqueous Solution," *Agro-Environmental Protection*, vol. 21, 2002.

[3] A. M. Abeish, H. M. Ang, and H. Znad, "Solar photocatalytic degradation of chlorophenols mixture (4-CP and 2,4-DCP): Mechanism and kinetic modelling," *Journal of Environmental Science and Health. Part A, Toxic/Hazardous Substances & Environmental Engineering*, vol. 50, no. 2, pp. 125–134, 2015.

[4] G. Qu, X. Wang, F. Li, and R. Pan, "Content analysis of dichlorobenzene in manufactured separate process," *Chemical Engineer*, vol. 9, pp. 21-22, 2007.

[5] C. Hou, X. Ge, Y. Zhou, Y. Li, D. Wang, and H. Tang, "Characterization of nanoscale iron and its degradation of 2, 4-dichlorophenol," *Chinese Science Bulletin*, vol. 54, 2009.

[6] P. Zhang, "Removal of 2,4-dichlorophenol from Aqueous Solution by Chitosan/Activity Carbon Fiber/TiO2 Composite Membrane," in *Master degree*, Dalian University of Technology, 2009.

[7] J. Li, F. Gao, J. Chen, Y. Hua, Z. Peng, and J. Wang, "Inhibition of phenol and its derivatives on dehydrogenase activity and luminescent bacteria biotoxicity," *Journal of Shanghai Ocean University*, vol. 19, pp. 111–115, 2010.

[8] C. Ma, F. Wang, J. Lu, M. Li, and W. Zheng, "Studies on Electrochemical Oxidation Reaction of 2,4-Dichlorophenol on Pt Electrode," *Chemical Journal of Chinese Universities*, vol. 34, pp. 2850–2854, 2013.

[9] Y. Ma, J. Chen, J. Yang, X. Song, H. Chen, and C. Gao, "The Advances of Research on Photocatalytic Oxidation of 2,4-Dichlorophenol," *Guangdong Chemical Industry*, vol. 43, pp. 86-87, 2016.

[10] X. Luo, S. Fu, and C. Zhou, "Photocatalytic degradation of 2,4-dichlorophenol using nanometer TiO2 on modified bamboo charcoal," *Journal of Zhejiang Forestry College*, vol. 24, pp. 524–527, 2007.

[11] M. Mohammadi and S. Sabbaghi, "Photo-catalytic degradation of 2,4-DCP wastewater using MWCNT/$TiO_2$ nano-composite activated by UV and solar light," *Environmental Nanotechnology, Monitoring & Management*, vol. 1-2, pp. 24–29, 2014.

[12] Y. Yang, Z. Sun, and Y. Chen, "Photocatalytic degradation of phenol and chlorinated phenols using nanometer TiO2 thin films," *Acta Energies Solaris Sinica*, vol. 25, pp. 63–67, 2004.

[13] B. Bayarri, J. Gimenez, D. Curco, and S. Esplugas, "Photocatalytic degradation of 2,4-dichlorophenol by $TiO_2$/UV: kinetics, actinometries and models," *Catalysis Today*, vol. 101, no. 3-4, pp. 227–236, 2005.

[14] D. Chen, Q. Zhu, F. Zhou, X. Deng, and F. Li, "Synthesis and photocatalytic performances of the $TiO_2$ pillared montmorillonite," *Journal of Hazardous Materials*, vol. 235-236, pp. 186–193, 2012.

[15] U. Pal, S. Ghosh, and D. Chatterjee, "Effect of sacrificial electron donors on hydrogen generation over visible light–irradiated nonmetal-doped TiO2 photocatalysts," *Transition Metal Chemistry*, vol. 37, pp. 93–96, 2011.

[16] D. Zhang, "Enhanced photocatalytic activity for titanium dioxide by co-modification with copper and iron," *Transition Metal Chemistry*, vol. 35, no. 8, pp. 933–938, 2010.

[17] D. Chatterjee, S. K. Moulik, L. Giribabu, and R. K. Kanaparthi, "Dye sensitization of a large band gap semiconductor by an iron(III) complex," *Transition Metal Chemistry*, vol. 39, no. 6, pp. 641–646, 2014.

[18] X. Li and C. Yang, "A Study of Photocatalytic Property of Nanosized TiO2," *Journal of China Three Gorges University (Natural Sciences)*, vol. 30, 2008.

[19] C. Yang, "Synthesis of mesoporous oxides and their use in efficient removal of fluoride from aqueous solution," in *Doctorate*, The China University of Geosiences at Wuhan, 2011.

[20] C. Li, R. Wang, X. Lu, and M. Zhang, "Mineralogical characteristics of unusual black talc ores in Guangfeng County, Jiangxi Province, China," *Applied Clay Science*, vol. 74, pp. 37–46, 2013.

[21] J. Zhou, "Hierarchically Porous Layered Double Hydroxides: hydrothermal synthesis and adsorption performance," in *Master degree*, Wuhan University of Technology, 2015.

[22] H. Hazwani Dzulkafli, F. Ahmad, S. Ullah, P. Hussain, O. Mamat, and P. S. M. Megat-Yusoff, "Effects of talc on fire retarding, thermal degradation and water resistance of intumescent coating," *Applied Clay Science*, vol. 146, pp. 350–361, 2017.

[23] W. L. Qin, H. Lv, T. Xia, Y. Ye, X. G. Chen, and S.S. Lyu, "$TiO_2$ intercalated talc nanocomposite: preparation, characterization, and its photocatalytic performance," *Journal of Nanoscience and Nanotechnology*, vol. 17, no. 9, pp. 6558–6565, 2017.

[24] Y. Liu, F. Yang, J. Pang, and J. Li, "Study on Properties of PP/SBS/Talc Ternary Composite," *Plastics Science and Technology*, vol. 44, pp. 31–34, 2016.

[25] H. Yang, J. Cao, A. Tang, W. Yang, and Y. Hu, "sothermal Crystallization Kinetics of Polypropylene/Talc Composites," *Journal of Plastics*, vol. 18, pp. 16–19, 2004.

[26] D. Yin and H. Tan, "Application Characteristics and Surface Modification of Talcum," *Guangdong Chemical Industry*, vol. 40, pp. 75–77, 2013.

[27] J. Tang, Y. Wang, A. Deng, H. Yuan, and K. Zhou, "Preparation and characterization of N-doped TiO2 photocatalyst," *The Chinese Journal of Nonferrous Metals*, vol. 17, pp. 1555–1560, 2007.

[28] G. Xu, M. Lu, and G. Sun, "Preparation and characterization of N–Ti-MCM-22 mesoporous molecular sieve and investigation of its photocatalytic properties," *Transition Metal Chemistry*, vol. 37, no. 3, pp. 235–240, 2012.

[29] M. Mirzaei, S. Sabbaghi, and M. M. Zerafat, "Photo-catalytic degradation of formaldehyde using nitrogen-doped $TiO_2$

nano-photocatalyst: Statistical design with response surface methodology (RSM)," *The Canadian Journal of Chemical Engineering*, vol. 96, no. 12, pp. 2544–2552, 2018.

[30] M. Salehi Morgani, R. Saboori, and S. Sabbaghi, "Hydrogen sulfide removal in water-based drilling fluid by metal oxide nanoparticle and $ZnO/TiO_2$ nanocomposite," *Materials Research Express*, vol. 4, no. 7, article 075501, 2017.

[31] W. Zhang, J. Yang, and C. Li, "Role of thermal treatment on sol-gel preparation of porous cerium titanate: characterization and photocatalytic degradation of ofloxacin," *Materials Science in Semiconductor Processing*, vol. 85, pp. 33–39, 2018.

[32] W. Zhang, Y. Tao, and C. Li, "Sol-gel synthesize and characterization of $_XGd_2Ti_2O_7/SiO_2$ photocatalyst for ofloxacin decomposition," *Materials Research Bulletin*, vol. 105, pp. 55–62, 2018.

[33] W. Zhang, F. Bi, Y. Yu, and H. He, "Phosphoric acid treating of ZSM-5 zeolite for the enhanced photocatalytic activity of $TiO_2$/HZSM-5," *Journal of Molecular Catalysis A: Chemical*, vol. 372, pp. 6–12, 2013.

[34] W. Zhang, Y. Liu, X. Pei, and X. Chen, "Effects of indium doping on properties of xIn-0.1%Gd-$TiO_2$ photocatalyst synthesized by sol-gel method," *Journal of Physics and Chemistry of Solids*, vol. 104, pp. 45–51, 2017.

[35] N. A. El-Zaher, M. S. Melegy, and O. W. Guirguis, "Thermal and structural analyses of PMMA/$TiO_2$ nanoparticles composites," *Natural Science*, vol. 6, no. 11, pp. 859–870, 2014.

[36] N. Mohajeri, A. T-Raissi, and J. Baik, "TG/DTA of hydrogen reduction kinetics of $TiO_2$ supported PdO chemochromic pigments," *Thermochimica Acta*, vol. 518, no. 1-2, pp. 119–122, 2011.

[37] T. Fu, X. Ling, Y. Ding, X. Zhu, H. Yang, and J. Zhu, "Adsorption Performance Analysis of Modified Mesoporous Carbon on Three Indexs in Drinking Water," *Environmental Science & Technology*, vol. 40, pp. 49–54, 2017.

[38] K. S. Sing, D. H. Everett, R. A. W. Haul et al., "Reporting Physisorption Data for Gas/Solid Systems with Special Reference to the Determination of Surface Area and Porosity," *Pure and Applied Chemistry*, vol. 57, pp. 603–619, 1984.

[39] X. Wei, K. Zhu, H. Wang, J. Yang, and J. Ma, "Study on Absorption of 2,4-Dichlorophenol with Modified Zeolites," *Journal of Safety and Environment*, vol. 3, pp. 57–59, 2003.

[40] L. Wang, W. Zhang, G. Song, J. Zhu, and Z. Peng, "Research of Degradation of 2,4-Dichlorophenol by Photocatalysis in Buffer Solution," *Journal of Qing Dao University*, vol. 27, pp. 27–30, 2014.

[41] Y. Zhang, H. Yang, S. Yan, J. Shen, and J. Liu, "Determination of Resorcinol Purity in the Hydrolysate of m -Dichlorobenzene by High Performance Liquid Chromatography," *Journal of Jiangsu Polytechnic University*, vol. 19, pp. 12–14, 2007.

[42] E. Pino and M. V. Encinas, "Photocatalytic degradation of chlorophenols on $TiO_2$-325mesh and $TiO_2$-P25. An extended kinetic study of photodegradation under competitive conditions," *Journal of Photochemistry and Photobiology A: Chemistry*, vol. 242, pp. 20–27, 2012.